ACS APPLIED MATERIALS & INTERFACES

Research Article

www.acsami.org

Ni-Doped Graphene/Carbon Cryogels and Their Applications As Versatile Sorbents for Water Purification

Gao Wei,[†] Yue-E Miao,[†] Chao Zhang,[†] Zhe Yang,[†] Zhenyan Liu,[†] Weng Weei Tjiu,[‡] and Tianxi Liu*[,†]

[†]State Key Laboratory of Molecular Engineering of Polymers, Department of Macromolecular Science, Fudan University, Shanghai 200433, P. R. China

[‡]Institute of Materials Research and Engineering, A*STAR (Agency for Science, Technology and Research), 3 Research Link, Singapore 117602, Singapore

Supporting Information

ABSTRACT: Ni-doped graphene/carbon cryogels (NGCC) have been prepared by adding resorcinol and formaldehyde to suspension of graphene oxide (GO), using Ni^{2+} ions as catalysts for the gelation process to substitute the usually used alkaline carbonates. The metal ions of Ni^{2+} have elevated the cross-linking between GO and RF skeletons, thus strengthening the whole cryogel. The as-formed three-dimensional (3D) interconnected structures, which can be well-maintained after freeze-drying of the hydrogel precursor and subsequent carbonization under an inert atmosphere, exhibit good mechanical properties. During the carbonization process, Ni^{2+} ions are converted into Ni nanoparticles and thus embedded in the interconnected structures. The unique porosity within the interconnected structures endows the cryogels with good capability for the extraction of oils and some organic solvents while the bulk form enables its recycling use. When ground into powders, they can be used as adsorbents for dyestuffs. Therefore, the as-obtained cryogels may find potential applications as versatile candidates for the removal of pollutants from water.

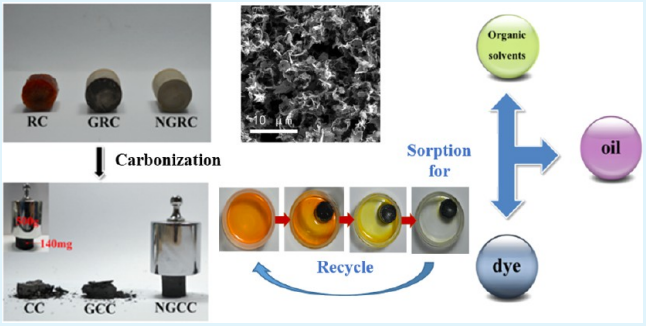

KEYWORDS: *graphene, carbon cryogels, Ni doping, water purification*

1. INTRODUCTION

Carbon aerogels, one kind of macroscopic porous material, prepared by the pyrolysis of alkaline carbonate (Na_2CO_3) catalyzed resorcinol (R)−formaldehyde (F) or phenol−furfural aerogels under an inert atmosphere, have a network structure of zero-dimensional interconnected nanoparticles.[1,2] They have received considerable attention in the fields of adsorption,[3] catalysis,[4] energy storage,[5] and so on, due to their low mass density, continuous porosity, high surface area, and high electrical conductivity. However, the wide applications of carbon aerogels are hampered by the extremely high expense of a supercritical drying technique used in the fabrication process.[6] Hence, a low-cost and easy-operation freeze-drying technique was developed to substitute the supercritical drying process, thus obtaining cryogels.[7−9] Nevertheless, the freeze-drying process always leads to brittle or broken samples, making it particularly difficult to obtain monoliths,[10] and methods like solvent exchange do not always solve the problem. Therefore, seeking approaches to preserve the structure of cryogels will greatly boost their applications.

Lately, two-dimensional (2D) graphene, with outstanding properties,[11,12] has been designed as a building block and integrated into 3D materials. Since Wang used noble metal salts to promote the macroassembly of single layered graphene in the presence of glucose,[13] various methods such as convenient hydrothermal[14] or chemical reduction[15] have been developed for the fabrication of graphene-based 3D assemblies. By the easy stacking of graphene layers, these 3D architectures usually appear as macroscopic, large-size monolithic materials which have tunable hierarchical morphologies and high surface areas.[16] In this way, phenomena at the nanoscale could be translated to the macroscopic level, paving the way to realizing novel applications of graphene based materials as adsorbents,[17] energy storage devices,[18] and scaffolds for cell growth.[19] Recent studies have reported macroscopic carbon cross-linked graphene composites and their applications in electrochemical areas.[20−22]

In the formation of these porously structured carbon materials, metal plays the important role of skeleton, filler, and linker. Some divalent metal ions (such as Ca^{2+}, Co^{2+}, Ni^{2+}) can perform as connecting agents in the 3D graphene oxide (GO) based materials, which can elevate the chemical cross-linking between graphene sheets.[23] Furthermore, transition metal salts, like those of Ni and Co, can tune the pore textures and surface characteristics of RF based carbon aerogels and induce the graphitization of resultant carbon aerogels when they substitute the usually used catalyst of Na_2CO_3 in the original recipes, and

Received: May 18, 2013
Accepted: July 15, 2013
Published: July 15, 2013

   dx.doi.org/10.1021/am401887g | ACS Appl. Mater. Interfaces 2013, 5, 7584−7591

the obtained transition metal containing carbon aerogels are essentially highly porous solids in the macroporous range.[24−27]

Oil spillage, toxic dyestuff, and organic solvent discharged from various industries are primary pollutants for water resources, posing a great threat to ecosystem and human health.[28,29] Thus, the development of novel and sustainable sorbents with low cost and high efficiency and versatility is urgently needed. Three-dimensional hydrophobic carbonaceous materials with well-developed porosity are ideal sorbents,[30−32] such as the flexible carbon nanofiber (CNF) aerogels recently reported by Yu et al. with outstanding sorption capability for removing a wide range of pollutants from water.[33,34] In this work, we report a unique strategy for preparing Ni-doped graphene/carbon cryogels (NGCC) by directly using GO sheets as templates for the growth of RF. Lewis acidic metal ions perform as both catalysts and cross-linkers due to their well-known ability to bind readily to oxygen groups.[35] The strong interactions among GO sheets and the cross-linking effect of the doped Ni can greatly strengthen the polymer framework, making the resultant monoliths able to maintain the interconnected structure during a freeze-drying process. The cryogels can be changed into carbonaceous bulk materials with hydrophobicity and porosity via pyrolysis. And they can be used as recyclable absorbents for oil and organic solvent spillage. When broken into powders, the adsorption capacity of the prepared cryogels to remove methyl blue (MB) from aqueous solution is also investigated.

2. EXPERIMENTAL SECTION

2.1. Materials. Natural graphite powder (325 mesh) was obtained from Alfa Aesar and used without further purification. Resorcinol, 37% formaldehyde, 98% H_2SO_4, $KMnO_4$, $NaNO_3$, and HCl were purchased from China Medicine Co. and used as received. 30% H_2O_2 was supplied by Jiangsu Tongsheng Chemical Reagent Company. $NiCl_2{\cdot}6H_2O$ was commercially received from Aldrich. Methyl blue (MB) was obtained from Sinopharm Chemical Reagent Co., Ltd. Deionized (DI) water was used as the solvent throughout the experiments.

2.2. Preparation of Graphite Oxide. Graphite oxide was prepared from natural graphite according to a modified Hummer's method. A 2.5 g portion of graphite powder was mixed with 1.25 g $NaNO_3$ and 115 mL of 98% H_2SO_4, followed by magnetic stirring in an ice-salt bath for 30 min. Then, 7.5 g of $KMnO_4$ was slowly added into the mixture under vigorous stirring for 2 h at a temperature below 20 °C. Successively, the reaction system was transferred to a 35 ± 3 °C flask in a water bath and kept there for 30 min. Then, 115 mL of DI water was added, sequenced by heating up the water bath to 98 °C and retaining for 15 min. The thick paste was diluted by adding 350 mL of DI water. Then, 30% H_2O_2 was added dropwise until the color of the mixture was changed from drab to brilliant yellow. Then, the suspension was filtered and washed by 800 mL 5% HCl and 300 mL DI water sequentially to remove metal ions, SO_4^{2-}, and H^+. Finally, the filter cake was dried in a vacuum oven at 50 °C overnight to obtain graphite oxide solid.

2.3. Synthesis of Ni-Doped Graphene/Carbon Cryogels (NGCC). The exfoliation of graphene oxide (GO) was carried out by ultrasonicating the graphite oxide in DI water for 2 h. Monolayer GO sheets with uniform thickness formed in the colloidal suspension (Supporting Information Figure S1). $NiCl_2{\cdot}6H_2O$ (20 mg) was dissolved in the exfoliated GO suspension (1 mg/mL, 20 mL) as the source of Ni^{2+}, 0.495 g resorcinol, and 0.73 g 37% formaldehyde were then added at a molar ratio of 1:2. After stirring to form a homogeneous solution, the mixture was cast into a glass mold. It was kept for curing at a temperature of 85 °C until a light brown-colored hydrogel was formed. After washing with DI water to remove the residue ions, it was lyophilized for several days at a temperature of −43 °C and vacuum of 10 Pa to get a Ni-doped GO/RF cryogel (NGRC). The cryogel was heated up to 950 °C at a heating rate of 10 °C/min under N_2 atmosphere and, then, kept for 2 h for carbonization and cooled naturally in a quartz tube furnace, and finally, a Ni-doped graphene/carbon cryogel (NGCC) was obtained.

To investigate the influence of Ni^{2+} ions on the formation of this 3D carbonaceous material, the GO/RF cryogel (GRC) was fabricated by using similar procedures except that no Ni^{2+} was added prior to the gelation step, and after carbonization, graphene/carbon cryogel (GCC) was obtained without Ni doping. A typical RF cryogel (RC) was also synthesized as a blank reference by using Na_2CO_3 as catalyst with an R/catalyst feed molar ratio of 200, it was then pyrolyzed into carbon cryogel (CC).

2.4. Characterization. Fourier transform infrared (FT-IR) spectra of the samples were measured with a Nicolet 6700 FT-IR spectrometer. X-ray diffraction (XRD) patterns of the samples were conducted on an

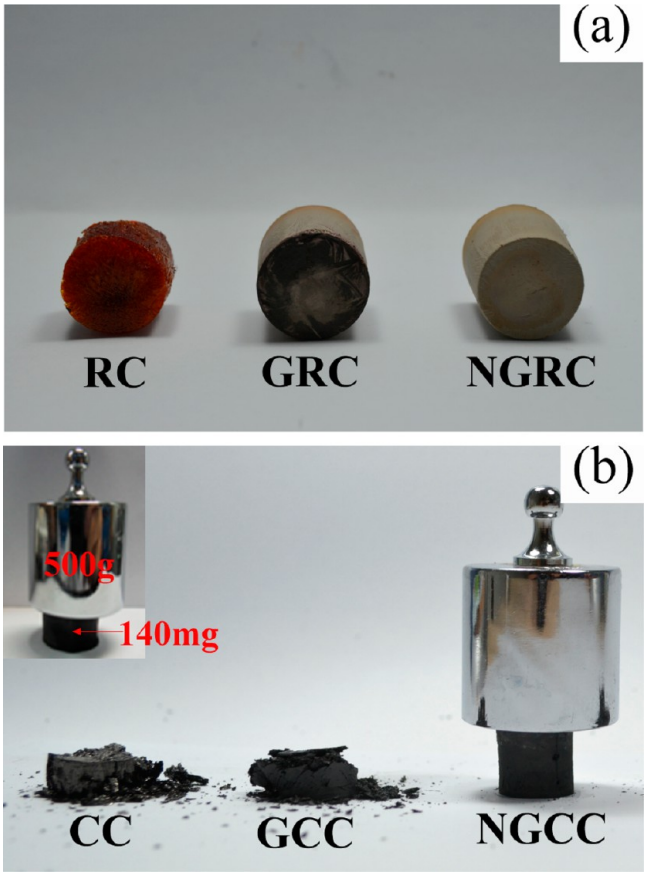

Figure 1. (a) Digital photographs of RC, GRC, and NGRC. Both GRC and NGRC are prepared with 1 mg/mL GO aqueous solution. (b) Digital photographs of CC, GCC, and NGCC with the same weight (90 mg) after loading with 200 g weight. (inset) 140 mg NGCC monolith enduring a weight of 500 g.

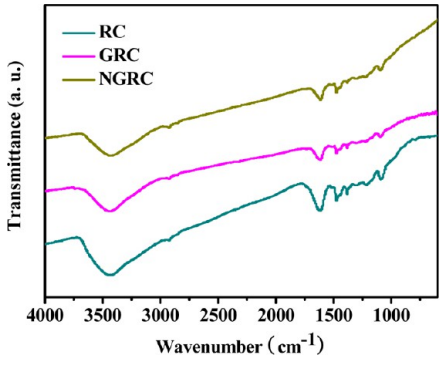

Figure 2. FTIR spectra of RC, GRC, and NGRC.

dx.doi.org/10.1021/am401887g | ACS Appl. Mater. Interfaces 2013, 5, 7584−7591

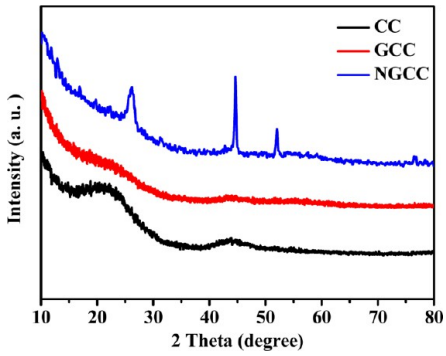

Figure 3. XRD patterns of CC, GCC, and NGCC.

X' Pert Pro X-ray diffractometer with Cu Kα radiation (λ = 0.1542 nm) under a voltage of 40 kV and a current of 40 mA. Scanning electron microscopy (SEM) images were acquired using a JEOL JSM-7600F with all samples coated with a thin layer of gold prior to SEM observation. Transmission electron microscopy (TEM) observation was performed with a Jeol 2100 TEM under an accelerating voltage of 200 kV coupled with an energy-dispersive X-ray (EDX) detector. Samples for TEM observations were prepared by dropping the solutions on the copper grids and drying in air. UV−vis absorption spectra were recorded on a Lambda 35 spectrometer (Perkin-Elmer). AFM imaging was performed by standard procedures in tapping mode on a Nanoscope IV scanning force microscope. Compressive tests were performed on Instron 5661 tester (compress rate = 0.005 s^{-1}). The specific surface area, pore size distribution, and pore volume were characterized with Tristar3000. Static contact angles were measured by using a commercial drop shape analysis system (Data Physics SCA20, Germany).

2.5. Absorption Experiments for Spoiled Oil and Organic Solvents. In the oil absorption tests, motor oil and vegetable oil (dyed with Aniline Yellow) were used as absorbates. The initial weight of monolithic cryogels before being immersed in the oil was recorded as

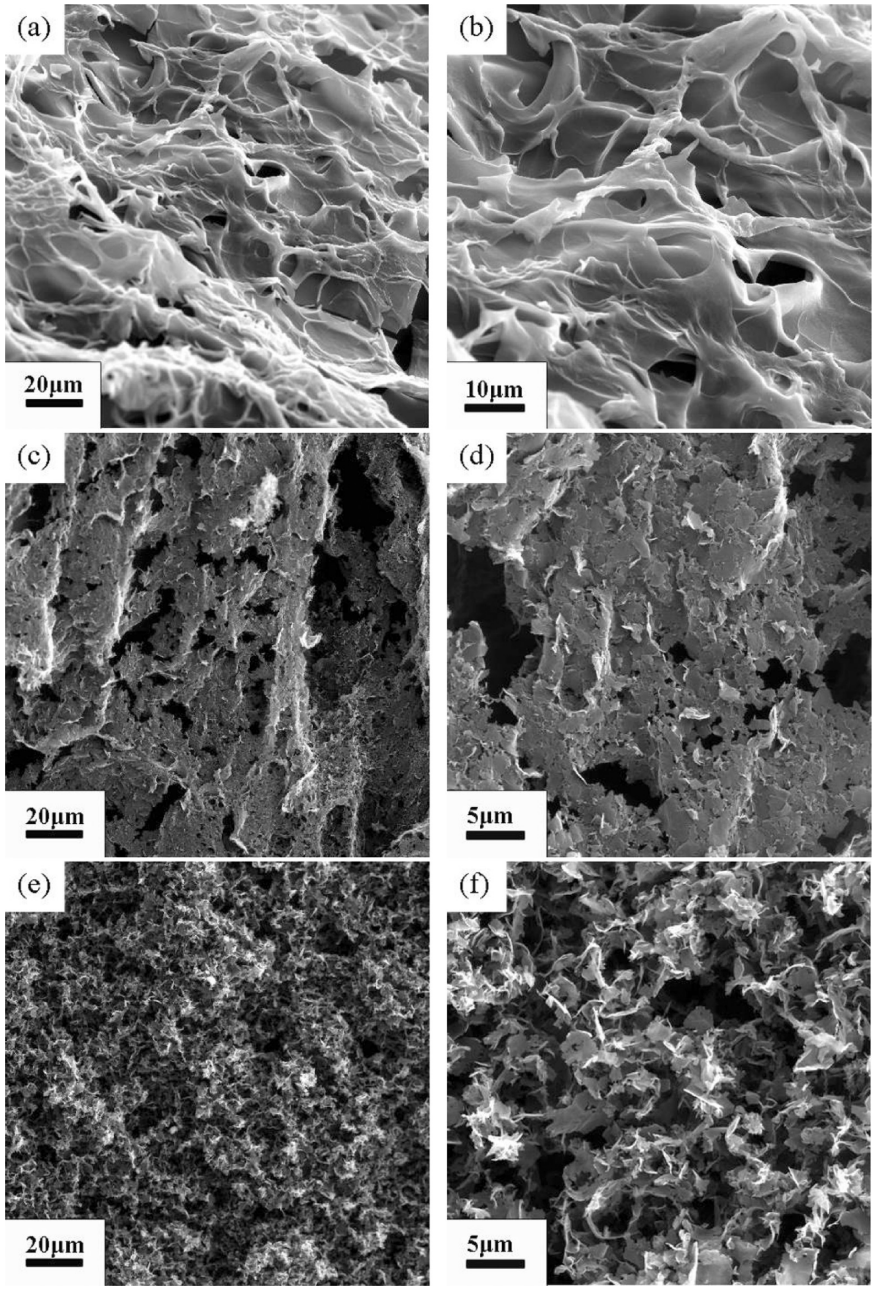

Figure 4. SEM images at low and high magnifications of CC (a and b), GCC (c and d), and NGCC (e and f).

M_0. After contact with the oil, the cryogels became saturated quickly in less than 1 min. They were taken out for weighing again after absorption with the terminal weight recorded as M_t. The oil absorption capacity of the cryogels was calculated and estimated using the following equation:

$$\text{oil absorption capacity (g/g)} = (M_t - M_0)/M_0$$

For recycling use, the absorbed oil was extracted by repeatedly soaking monolithic cryogels in the solvent of *n*-hexane for several hours. Until no oil entered the organic phase from the pores, the cryogels were withdrawn and heated up to 60 °C for the evaporation of residual *n*-hexane. Then, they were ready for the next cycle of absorption experiment. The absorption capacity measurements for organic solvents were conducted in the same way.

2.6. Adsorption Experiments for MB. MB stock solutions with a range of concentrations were prepared by dissolving MB in DI water. Batch adsorption experiments for MB were carried out in glass vessels at ambient temperature. The cryogels were broken into powders prior to the adsorption experiments. A certain amount of cryogel powders were added into MB solution, kept under magnetic stirring. For each sample, 0.5 mL solution was carefully withdrawn from the glass vessels at a predetermined time interval of 10 min and centrifuged to get the supernatant. The removal amount of MB was monitored by UV−vis spectroscopy equipped with a quartz cell of 1.0 cm path length. The UV−vis spectra of MB were recorded from 500 to 800 nm.

3. RESULTS AND DISCUSSION

3.1. Morphology and Structure of Cryogels. Figure 1a is the digital photograph of RF cryogel (RC), GO/RF cryogel (GRC), and Ni-doped GO/RF cryogel (NGRC). They are synthesized by curing the initial suspensions and subsequent freeze-drying of the corresponding hydrogels to remove the water inside, resulting in dried monoliths with shapes in accordance with the glass molds. It can be seen that RC is a brownish red cylinder with a loose structure, and visible channels caused by the sublimate in the drying process can be observed. After GO is introduced, even without adding Na_2CO_3 as catalyst, GRC can be obtained with a well-preserved structure due to the interaction among GO sheets. However, the bottom of the GRC still exhibits some black color which is different from the upper body, indicating nonuniformity of the bulk material. For NGRC, when metal salt of Ni^{2+} is used to promote the gelation process of GO/RF, Ni^{2+} ions are chelated by the negatively charged functional groups of RF and GO sheets, performing as cross-linking agents and catalyst at the same time, and thus, a homogeneous brownish−yellow monolith is formed. After pyrolysis under the N_2 atmosphere, RC, GRC, and NGRC are carbonized and converted into CC, GCC, and NGCC, respectively. Figure 1b illustrates the mechanical property of the as-obtained CC, GCC, and NGCC. It can be seen that NGCC, with doped Ni immobilized in its graphene/carbon networks, can endure more than 3500 times of its bulk weight without any deformation. The compressive stress−strain curves are shown in Supporting Information Figure S2. The compressive modulus of NGCC is calculated to be 0.95 MPa, while its compressive strength is 0.038 MPa, higher than the other two samples, indicating that it has a much better structural stability than the GCC and the very fragile CC.

Figure 2 presents the FT-IR spectra of the RC, GRC, and NGRC before carbonization. All of these three cryogels show the following similar characteristics. The absorption peaks at 2923 and 2854 cm^{-1} are respectively ascribed to the stretching vibration of CH_3- and CH_2- groups, while the 1475 cm^{-1} absorption band is assigned to CH_2-scissor vibration and CH_3-flexural vibration. The bands at 3440 and 1384 cm^{-1} are respectively attributed to the stretching and bending vibration of

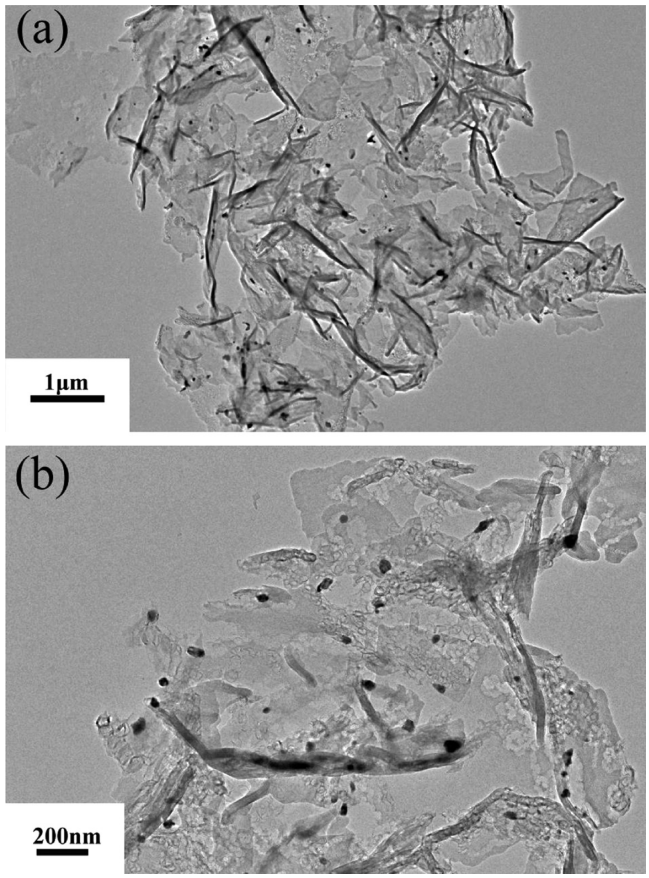

Figure 5. TEM images of NGCC at low (a) and high (b) magnifications.

O−H groups, which are derived from the C−OH as well as the trace of water in the pores of the cryogels. The band at 1614 cm^{-1} belongs to the stretching vibration of aromatic rings. The bands observed at 1095 and 1220 cm^{-1} are assigned to the methylene−ether (CH_3-O-CH_3), which is formed as a cross-linking bond between aromatic rings. IR measurements prove that the polymerization of RF occurs in all these three systems.[36] The oxygen-containing groups in the organic cryogels are eliminated by the calcination under inert atmosphere to achieve carbonaceous cryogels.

XRD patterns of the samples are depicted in Figure 3. CC presents a broad peak centered at $2\theta = 23.5°$, indicating a typical pattern of an amorphous carbon structure. A much narrower diffraction peak at $2\theta = 26.2°$ corresponding to the (002) of carbon is observed in NGCC, which can be attributed to the graphitization of amorphous carbon catalyzed by transition metal[37] and the change of the interlayer spacing.[38] The effect of transition metal was further proved by the XRD pattern of GCC as a control sample without adding Ni^{2+}, in which only a diffraction hump was observed in the 2θ range of 17° to 28°. All the three samples have a shoulder peak at $2\theta = 43.1°$, which is a fingerprint peak (101) for graphite. In NGCC, only strong diffraction peaks at $2\theta = 44.6°$, 51.9°, and 76.4° were observed together with those of graphite, being indexed as the (111), (200), and (220) crystal planes of face-centered cubic Ni (JCPDS card 65-2865). We can therefore confirm that Ni^{2+} ions were completely reduced to zero valence state after the calcination process.

Figure 4 shows the representative SEM micrographs of CC, GCC, and NGCC. For CC, it develops what is usually called

dx.doi.org/10.1021/am401887g | ACS Appl. Mater. Interfaces 2013, 5, 7584−7591

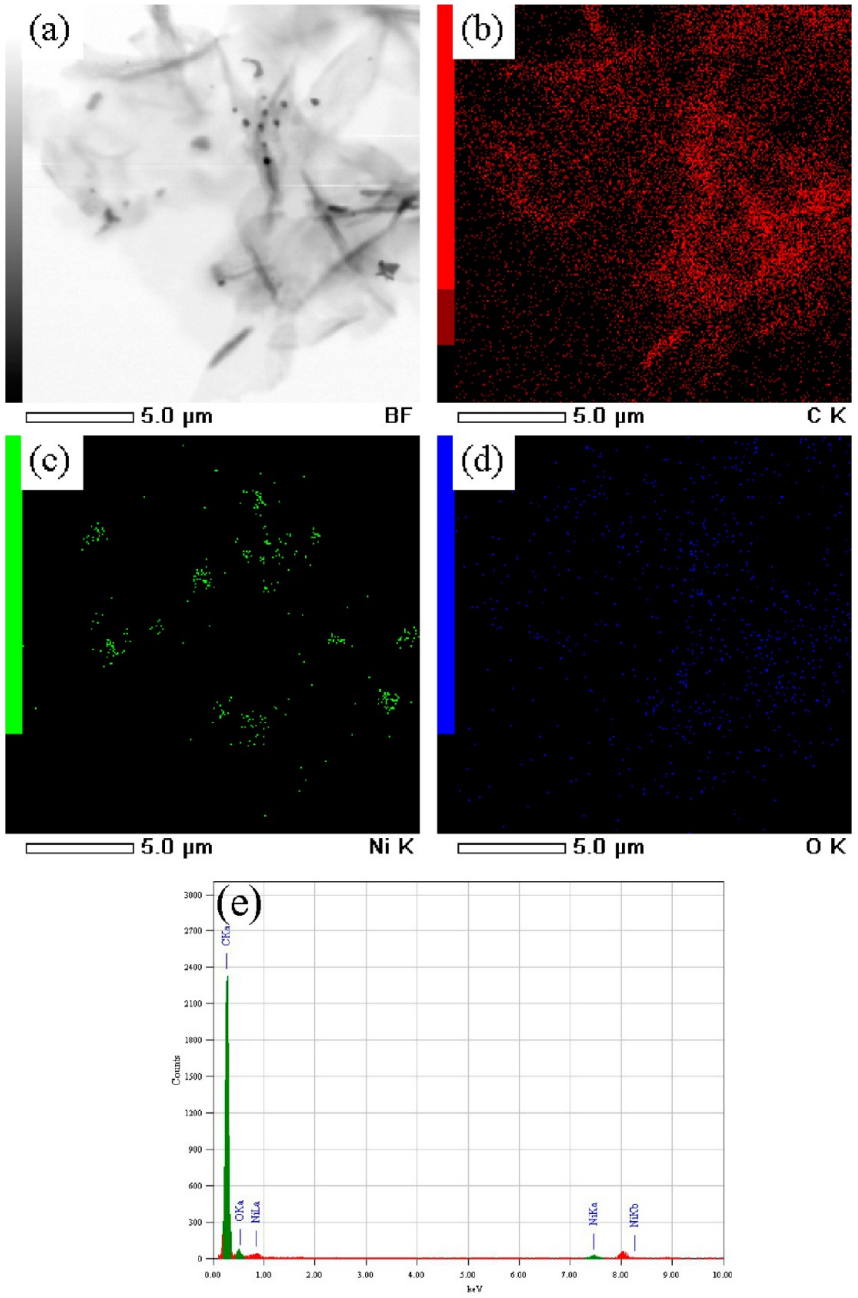

Figure 6. Bright field TEM image of NGCC (a) and its corresponding elemental mappings for C (b), Ni (c), and O (d). (e) The corresponding EDX spectrum taken from the whole area.

"megalopores" (Figure 4a and b). These very large pores are the remnant traces of ice crystals grown during the freezing drying process, and the sublimation of the ice also results in the collapse of its microstructure,[10] making the whole monolith fragile and inhomogeneous. For GCC, the SEM photographs show that thick layers comprised of closely packed carbon or graphene thin layers are formed (Figure 4c and d) as the exfoliated GO in the hydrogel precursor prefers to rearrange in a face-to-face way to stabilize the structure,[39] and the gradual growth of ice crystals during freeze-drying process also impels the overlap of the layers. However, this is not the case with NGCC, whose gelation process is facilitated by the presence of Ni^{2+}. As the metal ions can perform as cross-linkers, they provide active sites for the assembly of layers,[13] and many corrugations are formed in the Ni-bearing graphene/carbon cryogel, thus achieving a well-defined interconnected porous structure with the pore size ranging from submicrometers to tens of micrometers (Figure 4e and f). These phenomena demonstrate that the transition metal ions play an indispensable role in the assembly of graphene/carbon cryogel. The nitrogen-sorption isotherms and the BJH (Barret–Joyner–Halenda) desorption pore size distribution curve of NGCC are presented in Supporting Information Figure S3. The BET surface area is calculated to be 566.5 cm^2/g, and the pore volume is 0.577 cm^3/g, indicating that the cryogel can maintain a large surface area and good porosity after the freeze-drying process.

To further investigate the morphology, TEM photographs of NGCC powders are shown in Figure 5. It reveals that Ni nanoparticles are sparsely and randomly scattered throughout the carbonaceous matrix. In some locations, new types of nanostructure such as graphitic filaments and ribbons are obtained, which

dx.doi.org/10.1021/am401887g | ACS Appl. Mater. Interfaces 2013, 5, 7584–7591

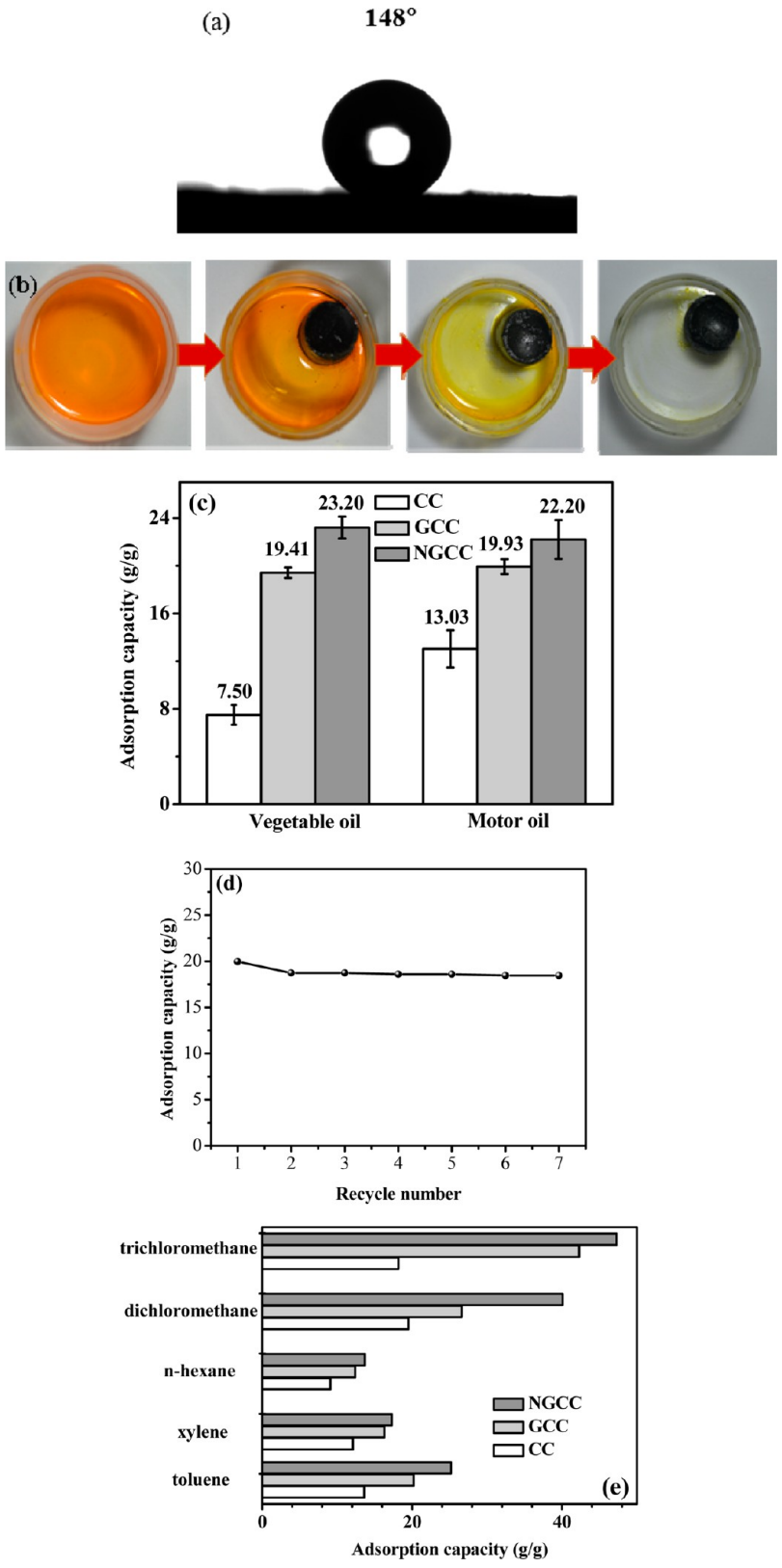

Figure 7. (a) Contact angle test of NGCC. (b) Digital photograph of the oil absorption by NGCC in 1 min. (c) The oil absorption capacity of CC, GCC, NGCC. (d) Recycling performance of the motor oil absorption capacity of NGCC. (e) The organic solvent adsorption capacity of CC, GCC, and NGCC.

may be formed by the graphitization of the carbonaceous matrix by transitional metal at a high temperature of carbonization.[40] The corresponding EDX elemental mapping is used to study elemental distribution in the cryogels as shown in Figure 6. It can be seen that the carbonaceous framework is decorated with some Ni-rich phase regions, showing a slight aggregation in some edge areas, which may be derived from the strong bonds between metal ions and the carboxylic acid groups at the edges of the individual GO sheets in

dx.doi.org/10.1021/am401887g | ACS Appl. Mater. Interfaces 2013, 5, 7584−7591

the initial suspension.[35] Although the EDX spectra also show the presence of oxygen, it just exists in trace amounts which can be attributed to the residual oxygen functional groups remaining on the substrate after calcination.

3.2. Oil and Organic Solvent Absorption Capacity of Cryogels. The absorption capacity for organic molecules is determined to a large extent by the characteristics of the absorbent and absorbate. The pore texture, surface chemistry, and mineral matter content have large effects on the absorption properties of the carbon materials. NGCC has a contact angle of 148° (Figure 7a), indicating that it has a hydrophobic surface. As shown in Figure 7b, the NGCC completes the absorption activity in 1 min due to the superwetting behavior for oils. When coming into contact with a layer of oil floating on the water surface, it repels the water phase and uptakes the oil due to its hydrophobic surface, making it an excellent alternative absorbent for the oil leakage treatment. Figure 7b demonstrates the uptake capacity of the three monolithic cryogels for vegetable and motor oil. As reported in previous studies, absorption mainly occurs in large pores and mesoporous structure of the porous materials.[41,42] As shown in the bar chart (Figure 7b), CC shows a low absorption capacity as its RF based porous carbon structure mostly collapses during the drying process. Compared with CC, the absorption capacity of GCC is greatly improved when GO is added to preserve the structure. However, when Ni^{2+} ions are used as cross-linkers in the system, the piled-up microstructure of GCC is changed into a well-developed porous structure constructed by the randomly orientated carbonaceous walls in NGCC. Thus NGCC has the highest oil uptake capacity (more than 20 times of its bulk weight) among these three cryogels. Figure 7c shows that 93% of the absorption capacity of monolithic NGCC for motor oil can be preserved even after seven cycles, implying good recycling performance. As shown in Figure 7d, the absorption capacity of the CC, GCC, and NGCC for a range of organic solvents is consistent with their uptake capacity for oils (Figure 7b). Several sorbents and their oil uptake capacities are listed in Table 1. Considering its apparent density (estimated to be 38 mg/cm^3), the NGCC has a comparable sorption capacity toward oils and organic solvents. Therefore, it should be a promising candidate in environment remediation.

Table 1. Comparison of Sorption Capacities of Different Sorbents

sample	oil	sorption capacity (g/g)	ref
BN nanosheets	engineering oil	29	43
organoclays	diesel	7.2	44
fir fibers	grade-C oil	15	45
corn stalk	gas oil	8	46
CNF aerogel	pump oil, gasoline	100−200	33
CNF aerogel	gasoline, vegetable oil	40−80	34
graphene/a-FeOOH aerogel	vegetable oil, gasoline	10−30	47
CNF/carbon foam	motor oil	25	48
CNT sponge	vegetable oil	32.3	49
NGCC	motor oil, vegetable oil	22.2−23.2	this study

3.3. MB Adsorption Using Carbonaceous Cryogels. Figure 8 illustrates the typical MB adsorption capacity−time curves of the powders derived from the as-obtained cryogels. The 3D structures are smashed during the grinding of these cryogels. Therefore, the effect of graphene on the dye adsorption behaviors for the CC and NGCC powdery samples were investigated. As for GCC, it has a nonuniform nature and is not considered here. It can be obviously seen that CC has a very low adsorption capacity, only reaching 12 mg/mL after 1 h adsorption (Figure 8a). For this kind of cryogel, the loss of pores caused by the freeze-drying method leads to the reduction of adsorption sites, thus resulting in the decrease of both adsorption capacity and efficiency. In contrast, for NGCC, the adsorption curves have already reached equilibrium in 10 min and plateaued afterward. The introduction of graphene greatly tunes the morphology of RF based cryogels, leading to enhanced surface areas and homogeneous porosities. And with a high degree of electron delocalization conjugated system on the surface area due to the sp^2 hybridization of carbon atoms, they are more inclined to couple with organic dye molecules. All of these factors contribute to a significant improvement in adsorption capacity of the hybrids. It is further confirmed by changing the content of graphene in the whole NGCC cryogel. The adsorption capacities of the resultant cryogels increase with the ascending feed ratios of GO in the initial solution, and the NGCC prepared with an initial GO concentration of 6 mg/mL (denoted as NGCC6) shows the highest MB adsorption capacity among all the samples investigated. A maximum adsorption capacity of 151 mg/g is calculated from the fitted Langmuir model (Supporting Information Figure S4 and Table S1).

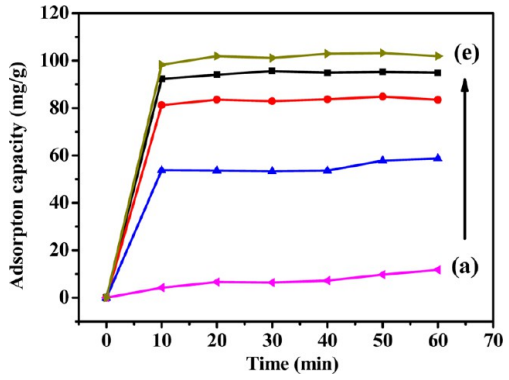

Figure 8. Adsorption curves of MB from aqueous solution by CC (a) and NGCC prepared from GO suspension with an initial concentration of 1 (b), 2 (c), 3 (d), and 6 mg/mL (e).

4. CONCLUSIONS

In this work, a simple approach has been proposed to prepare monolithic Ni-doped graphene/carbon cryogels (NGCC) with high mechanical strength. NGCC can keep unchangeable during the freeze-drying process without any pretreatments. The morphological and structural characterizations have confirmed that well-defined architectures with homogeneous porosity have been established for NGCC. The cryogel monoliths exhibit ultrafast absorption rate and high uptake capacity for oils and organic solvents with a good recyclability. Furthermore, the cryogels in the form of powders can be applied to quickly remove dyes from the aqueous solution. The excellent ability to eliminate various pollutants makes the NGCC cryogels useful candidates for water disposal. Herein, our work provides a simple way to broaden the application scope of low-cost carbonaceous cryogels by the remediation of their fragility and the incorporation of metal dopant.

■ ASSOCIATED CONTENT

Supporting Information

AFM image of graphene oxide monolayer (a) and the corresponding height profile (b); compressive stress−strain

curves of CC, GCC, and NGCC; the nitrogen-sorption isotherm and the BJH (Barret−Joyner−Halenda) desorption pore size distribution curve of NGCC (the inset is the cumulative pore volume−pore diameter curve); adsorption isotherm of NGCC prepared with 6 mg/mL GO concentration; Langmuir isotherm parameters for MB adsorption of NGCC. This material is available free of charge via the Internet at http://pubs.acs.org.

AUTHOR INFORMATION

Corresponding Author

*E-mail: txliu@fudan.edu.cn. Tel.: +86-21-55664197. Fax: +86-21-65640293.

Notes

The authors declare no competing financial interest.

ACKNOWLEDGMENTS

The authors are grateful for the financial support from the National Natural Science Foundation of China (51125011).

REFERENCES

(1) Al-Muhtaseb, S. A.; Ritter, J. A. *Adv. Mater.* **2003**, *15*, 101−114.
(2) Long, D.; Zhang, J.; Yang, J.; Hu, Z.; Li, T.; Cheng, G.; Zhang, R.; Ling, L. *New Carbon Mater.* **2008**, *23*, 165−170.
(3) Meena, A. K.; Mishra, G. K.; Rai, P. K.; Rajagopal, C.; Nagar, P. N. *J. Hazard. Mater.* **2005**, *122*, 161−170.
(4) Moreno-Castilla, C.; Maldonado-Hodar, F. J. *Carbon* **2005**, *43*, 455−465.
(5) Li, J.; Wang, X. Y.; Huang, Q. H.; Gamboa, S.; Sebastian, P. J. *J. Power Sources* **2006**, *158*, 784−788.
(6) Chaichanawong, J.; Yamamoto, T.; Kim, S. I.; Ohmori, T. *J. Non-Cryst. Solids* **2009**, *355*, 1605−1612.
(7) Tamon, H.; Ishizaka, H.; Yamamoto, T.; Suzuki, T. *Carbon* **1999**, *37*, 2049−2055.
(8) Tamon, H.; Ishizaka, H.; Yamamoto, T.; Suzuki, T. *Carbon* **2000**, *38*, 1099−1105.
(9) Yamamoto, T.; Nishimura, T.; Suzuki, T.; Tamon, H. *J. Non-Cryst. Solids* **2001**, *288*, 46−55.
(10) Job, N.; Théry, A.; Pirard, R.; Marien, J.; Kocon, L.; Rouzaud, J.; Béguin, F.; Pirard, J. *Carbon* **2005**, *43*, 2481−2494.
(11) Geim, A. K.; Novoselov, K. S. *Nat. Mater.* **2007**, *6*, 183−191.
(12) Rao, C.; Sood, A. K.; Subrahmanyam, K. S.; Govindaraj, A. *Angew. Chem., Int. Ed.* **2009**, *48*, 7752−7777.
(13) Tang, Z. H.; Shen, S. L.; Zhuang, J.; Wang, X. *Angew. Chem., Int. Ed.* **2010**, *49*, 4603−4607.
(14) Xu, Y. X.; Sheng, K. X.; Li, C.; Shi, G. Q. *ACS Nano* **2010**, *4*, 4324−4330.
(15) Sheng, K.; Xu, Y.; Li, C.; Shi, G. Q. *New Carbon Mater.* **2011**, *26*, 9−15.
(16) Zhao, Y.; Hu, C. G.; Hu, Y.; Cheng, H. H.; Shi, G. Q.; Qu, L. T. *Angew. Chem., Int. Ed.* **2012**, *51*, 11371−11375.
(17) Sui, Z. Y.; Meng, Q. H.; Zhang, X. T.; Ma, R.; Cao, B. *J. Mater. Chem.* **2012**, *22*, 8767−8771.
(18) Zhang, L.; Shi, G. Q. *J. Phys. Chem.* **2011**, *115*, 17206−17212.
(19) Lim, H. N.; Huang, N. M.; Lim, S. S.; Harrison, I.; Chia, C. H. *Int. J. Nanomed.* **2011**, *6*, 1817−1823.
(20) Worsley, M. A.; Pauzauskie, P. J.; Olson, T. Y.; Biener, J.; Satcher, J. H.; Baumann, T. F. *J. Am. Chem. Soc.* **2010**, *132*, 14067−14069.
(21) Zhang, K.; Ang, B. T.; Zhang, L. L.; Zhao, X. S.; Wu, J. S. *J. Mater. Chem.* **2011**, *21*, 2663−2670.
(22) Marković, Z. M.; Babić, B. M.; Dramićanin, M. D.; Holclajtner Antunović, I. D.; Pavlović, V. B.; Peruško, D. B.; Todorović Marković, B. M. *Synth. Met.* **2012**, *162*, 743−747.
(23) Jiang, X.; Ma, Y. W.; Li, J. J.; Fan, Q. L.; Huang, W. *J. Phys. Chem. C.* **2010**, *114*, 22462−22465.
(24) Maldonado-Hodar, F. J.; Moreno-Castilla, C.; Rivera-Utrilla, J.; Hanzawa, Y.; Yamada, Y. *Langmuir* **2000**, *16*, 4367−4373.
(25) Audier, M.; Oberlin, A.; Oberlin, M.; Coulon, M.; Bonnetain, L. *Carbon* **1981**, *19*, 217−224.
(26) Moreno-Castilla, C. F.; José Maldonado-Hódar, J.; Rivera-Utrilla, Rodríguez-Castellón, E. *Appl. Catal. A: Gen.* **1999**, *183*, 345−356.
(27) Maldonado-Hodar, F. J.; Ferro-Garcia, M. A.; Rivera-Utrilla, J.; Moreno-Castilla, C. *Carbon* **1999**, *37*, 1199−1205.
(28) Morais, L. C.; Freitas, O. M.; Gonçalves, E. P.; Vasconcelos, L. T.; González Beça, C. G. *Water Res.* **1999**, *33*, 979−988.
(29) Adebajo, M. O.; Frost, R. L.; Kloprogge, J. T.; Carmody, O.; Kokot, S. *J. Porous Mater.* **2003**, *10*, 159−170.
(30) Li, H.; Liu, L. F.; Yang, F. L. *J. Mater. Chem. A* **2013**, *1*, 3446−3453.
(31) Yang, W.; Wu, D.; Fu, R. *Colloids Surf., A* **2008**, *312*, 118−124.
(32) Wu, X.; Wu, D.; Fu, R. *J. Hazard. Mater.* **2007**, *147*, 1028−1036.
(33) Liang, H. W.; Guan, Q. F.; Chen, L. F.; Zhu, Z.; Zhang, W. J.; Yu, S. H. *Angew. Chem., Int. Ed.* **2012**, *51*, 5101−5105.
(34) Wu, Z. Y.; Li, C.; Liang, H. W.; Chen, L. F.; Yu, S. H. *Angew. Chem., Int. Ed.* **2013**, *52*, 2925−2929.
(35) Park, S.; Lee, K. S.; Bozoklu, G.; Cai, W.; Nguyen, S. T.; Ruoff, R. S. *ACS Nano* **2008**, *2*, 572−578.
(36) Li, W.; Lu, A.; Guo, S. *Carbon* **2001**, *39*, 1989−1994.
(37) Maldonado-Hódar, F. J.; Moreno-Castilla, C.; Pérez-Cadenas, A. F. *Microporous Mesoporous Mater.* **2004**, *69*, 119−125.
(38) Chen, W. F.; Yan, L. F. *Nanoscale.* **2011**, *3*, 3132−3137.
(39) Cote, L. J.; Kim, F.; Huang, J. X. *J. Am. Chem. Soc.* **2009**, *131*, 1043−1049.
(40) Fu, R. W.; Baumann, T. F.; Cronin, S.; Dresselhaus, G.; Dresselhaus, M. S.; Satcher, J. H. *Langmuir* **2005**, *21*, 2647−2651.
(41) Gui, X. C.; Wei, J. Q.; Wang, K. L.; Cao, A. Y.; Zhu, H. W.; Jia, Y.; Shu, Q. K.; Wu, D. H. *Adv. Mater.* **2010**, *22*, 617.
(42) Toyoda, M.; Nishi, Y.; Iwashio, N.; Inagaki, M. *Desalination* **2003**, *151*, 139−144.
(43) Lei, W. W.; Portehault, D.; Liu, D.; Qin, S.; Chen, Y. *Nat. Commun.* **2013**, *4*, 1777.
(44) Carmody, O.; Frost, R.; Xi, Y. F.; Kokot, S. *J. Colloid Interface Sci.* **2007**, *305*, 17−24.
(45) Inagaki, M.; Kawahara, A.; Konno, H. *Carbon* **2002**, *40*, 105−111.
(46) Husseien, M.; Amer, A. A.; El-Maghraby, A.; Hamedallah, N. *Anal. Appl. Pyrol.* **2009**, *86*, 360−363.
(47) Cong, H. P.; Ren, X. C.; Wang, P.; Yu, S. H. *ACS Nano* **2012**, *6*, 2693−2703.
(48) Xiao, N.; Zhou, Y.; Ling, Z.; Qiu, J. S. *Carbon* **2013**, *59*, 530−536.
(49) Gui, X. C.; Li, H. B.; Wang, K. L.; Wei, J. Q.; Jia, Y.; Li, Z.; Fan, L. L.; Cao, A. Y.; Zhu, H. W.; Wu, D. H. *Acta Mater.* **2011**, *59*, 4798−4804.